Dynamic fragmentation of single-walled carbon nanotubes induced by sonication

H.B. Chew, K.-S. Kim
Brown University, Providence, Rhode Island, USA

Abstract

Ultrasonication is widely recognized as a highly effective means of cutting long and entangled single-walled carbon nanotubes (SWCNTs) into shorter pieces. The exact nanotube cutting mechanism, however, remains elusive. While some have attributed the fragmentation process to the microscopic domains of high temperature that attacks the surface of the SWCNTs during bubble implosion, others have suggested that the large friction forces between the liquid and the SWCNTs resulted in the scission process. In this work, we use scale-bridging molecular dynamics simulations to ascertain the exact nanotube cutting mechanisms. Results show that friction forces alone are insufficient to fracture the nanotube. However, photon irradiation during the collapse of cavitation bubbles could induce the formation of significant proportions of defects in the SWCNTs: these defects contribute to both increased frictional loads, and reduced critical shell buckling loads, ultimately leading to nanotube scission.

1. Introduction

The synthesis of single-walled carbon nanotubes (SWCNTs) typically results in highly entangled nanotube ropes of lengths on the order of microns. However, the availability of individual shorter length nanotubes is essential in many specialized biological and technological applications, such as drug delivery, DNA analysis, molecular sensors, and high performance nanocomposites. To this end, researchers have proposed many physical and chemical methods to cut these as produced nanotube ropes into shorter individual pieces [1-6]. Of which, ultrasonication is perhaps the most effective means of dispersing and cutting SWCNTs in large quantities, with minimal carbon losses and recoverable sidewall damage.

Liu et al. [7] showed that prolonged sonication of nearly endless, highly entangled ropes of SWCNTs in a mixture of concentrated sulfuric and nitric acid, with the help of surfactants, resulted in short, open-ended pipes that behave as individual macromolecules. They suggested that the collapse of cavitation bubbles during ultrasonication produces microscopic domains of high temperature that attacks the surface of the SWCNTs, leaving an open hole in the tube side. The acid mixture then oxidizes the tube at this defect site and cuts the tube. More recently, Heller et al. [8] observed that individually dispersed SWCNTs in aqueous surfactant

suspensions could be cut by the sonication process used to disperse them. Using electrophoresis and column chromatography to sort the shortened nanotubes by length, Heller et al. found that sonication shortens larger diameter nanotubes more than smaller ones. Hennrich et al. [9] also noted similar diameter-dependent scission rate under ultrasonication, and proposed that the friction forces between the fluid and the nanotube could fracture the nanotube during bubble implosion. In this work, we attempt to ascertain the exact nanotube cutting mechanisms using scale-bridging molecular dynamics simulations.

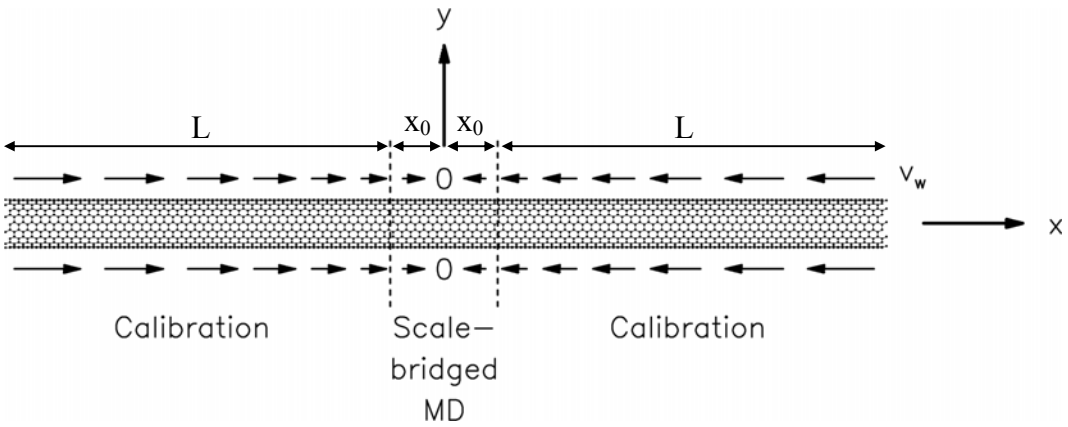

Figure 1. Schematic of the scale-bridged MD simulation model.

2. Length-scale-bridging molecular dynamics

For individually dispersed SWCNTs in aqueous surfactant suspensions subjected to ultrasonic treatment, incipient cavity bubbles likely nucleate on the hydrophobic nanotube sidewalls during the tensile phase of sound. At some instant during the sonic compression phase, the high surface tension drives the sudden collapse of the bubble to a fraction of its maximum size. Compared to the bubble's surface, the motion of the nanotube is slightly retarded due to its greater inertial mass, and the nanotube subsequently detaches from the bubble's surface. Bubble implosion then drives the fluid surrounding the nanotube inwards towards the nanotube's center with velocity

$$v_w = \dot{\varepsilon} x \tag{2.1}$$

where x represents the axial distance from the nanotube's center (see Fig. 1), and $\dot{\varepsilon}$ is the collapse strain rate close to the surface of a collapsing bubble which is on the order of -10^9 s^{-1} [10]. The induced frictional stress, τ, then drives the nanotube's subsequent compressive motion towards its center. Hence, by studying the relationship between τ and v_w, the distribution of τ along the nanotube can be obtained.

We set the wall boundary surrounding an infinitely long nanotube (periodic in the axial direction) to move with velocity v_w – this indirectly drives a Couette-like flow over the nanotube by virtue of shear deformation due to the nonslip wall

boundary condition. See Fig. 2. The periodic ends of the nanotube at the box boundary are rigidly constrained to resist the drag by the flow dynamics, while the remaining carbon atoms are free to vibrate in all directions, resulting in flexible nanotube sidewalls. The friction forces and hence τ are obtained by computing the total time averaged axial forces on the carbon atoms after steady-state flow has been achieved.

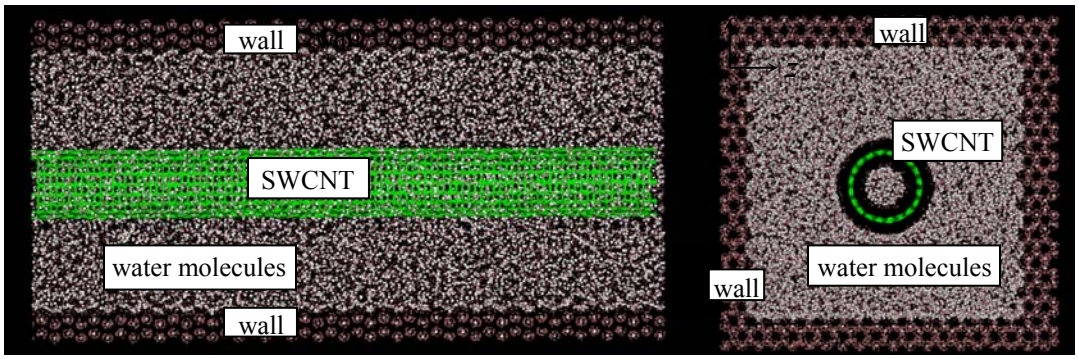

Figure 2. A (10,10) SWCNT surrounded by water molecules with axially moving wall boundary.

Considering just the positive end of the SWCNT (i.e. $x > 0$), the accumulated friction forces transmitted along the nanotube can then be expressed as

$$F(x) = -\pi D \int_x^L \tau(x) dx \tag{2.2}$$

where D and L represent the diameter and half-length of the SWCNT respectively. Equal and opposite forces act along the negative side of the SWCNT ($x < 0$). Since the length of an uncut SWCNT is on the order of microns, which is way too long to be handled by molecular dynamics, we effectively reduce the length-scale of simulation from μm to nm by imposing $F(x_0)$ from (2.2) at the boundary ends ($x = \pm x_0$) of the scale-bridged model of a length-scale suitable for MD simulations. We uniformly distribute $F(x_0)$ among the boundary atoms of the nanotube, and constrain these atoms to move only axially.

The carbon nanotube-water systems described above are modeled using the classical molecular dynamics simulation software package LAMMPS [11] in the micro canonical (NVE) ensemble. The interactions between carbon atoms are described by the adaptive intermolecular potential, AIREBO [12]. The water intramolecular potential is described using the TIP4P-Ew model [13]. The carbon-water interaction is described by a Lennard-Jones potential acting between the carbon atoms and the oxygen atoms, with a carbon-oxygen van der Waals radius of $\sigma_{CO} = 3.19\,\text{A}^\circ$ and a well-depth of $\varepsilon_{CO} = 0.3126\ \text{kJ mol}^{-1}$ [14]. The effective thickness of the nanotube is taken to be equal to the interlayer spacing in graphite, i.e. 0.34 nm, which is also inline with the AIREBO potential. The employed time

step is 1 *f*s. For all computations, the SWCNTs are surrounded by a water box of randomly distributed H_2O molecules with density ρ_w = 997 kg m^{-3}. An initial energy minimization of the system is performed, after which the system is equilibrated for 5 *p*s and the temperature is adjusted to the desired value of 300 *K* using velocity scaling. Thereafter during the production phase, the water bath in the system is coupled to a Berendsen thermostat [15] in order to avoid the effects of viscous heating.

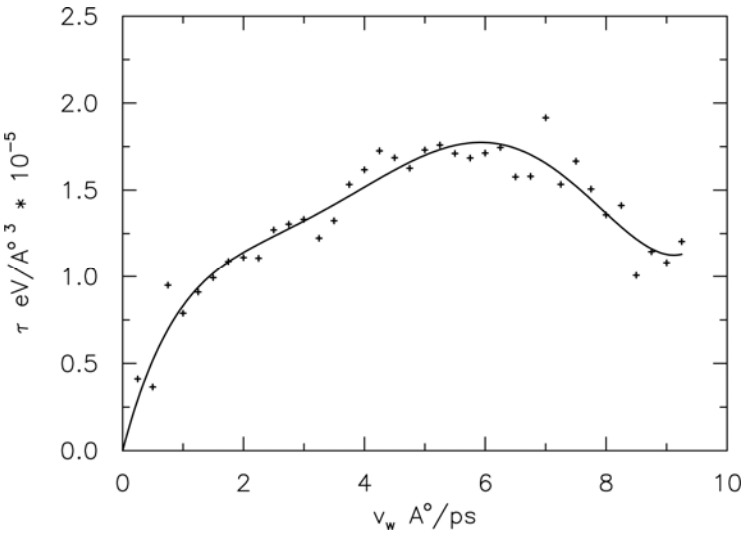

Figure 3. Profile of time-averaged frictional stress τ versus flow velocity v_w for the (10,10) SWCNT.

3. Results and discussions

We confine our study to a (10,10) open-end SWCNT. Fig. 3 shows the time-averaged frictional stress versus streaming velocity profile for the SWCNT. At low velocities of v_w < 1 A°/*p*s, the frictional stress increases almost linearly with v_w. At higher velocities, τ increases more slowly, reaching a peak at about v_w = 6 A°/*p*s. Further increase in v_w causes a reduction in τ. These trends are in sharp contrast to the linear frictional stress versus velocity predictions by continuum Navier-Stokes models. The discrepancy can be partly explained by the slip condition of the fluid at the hydrophobic wall-boundary of the SWCNT [16, 17]. Recent experiments have also showed that water on meeting a hydrophobic surface, forms a thermodynamically driven low-density depletion layer [18]. The strong hydrogen-bonding between water molecules causes the fluid to recede from nonpolar surfaces and form distinct layers separating the bulk phase from the surface [19]. Instead of entering the interstices, the fluid remains atop the carbon atoms (known as the Cassie state or Fakir effect), leading to very small liquid-solid contact area. In addition, the substantial drop in τ as v_w increases beyond 6 A°/*p*s can be attributed to the increasing effects of resonance as the streaming velocity approaches the vibrational wave speed of the nanotube.

From the calibration profile in Fig. 3, we subsequently obtain the accumulated frictional forces $F(x_0)$ to be applied at the scale-bridged ends of the nanotube using (2.1) and (2.2). The profiles for $F(x_0)$ versus the actual nanotube half-length L are displayed in Fig. 4. These frictional loads are compared against the critical buckling loads of the SWCNT.

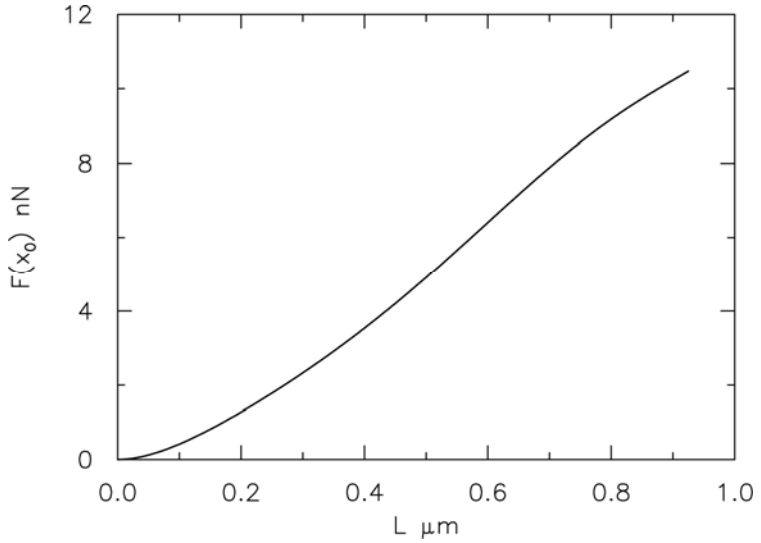

Figure 4. Profile of accumulated frictional forces $F(x_0)$ versus nanotube half-lengths L for the (10,10) SWCNT.

Since the duration of bubble implosion under ultrasonication is insufficient for Euler buckling of the SWCNT in water to occur, we postulate that shell buckling is the dominant failure mode leading to nanotube scission. With this in mind, we keep the aspect ratio x_0/D of the nanotube in our scale-bridged model sufficiently small to avoid triggering Euler buckling. The compressive forces applied at the ends of the scale-bridged model (at $x = \pm x_0$) are systematically increased until shell buckling of the nanotube occurs. The mode of deformation involves the formation of periodic arrays of azimuthal lobes and half waves throughout the nanotube, while maintaining the symmetry axis of the SWCNT. Our simulations show that the critical shell buckling load for a (10,10) SWCNT is around 58 nN, which is several-folds larger than $F(x_0)$ in Fig 4 over the range of nanotube lengths considered (compared to $F(x_0) = 11$ nN for 1.8 μm long SWCNT). Hence, frictional effects alone cannot account for the cutting of the nanotube.

During the sonic compression phase, the gas inside the imploded bubble is adiabatically compression and heated up to temperatures of around 5000 K [20]. If the insonation is sufficiently intense, flashes of light caused by the violent multiple bubble collapses are emitted – a phenomenon known as multiple bubble sonoluminescence. The spectra of multiple bubble sonoluminescence show that most of this emitted light is ultraviolet. In this regime ($\lambda = 200$ nm), the energy of each emitted photon is about 6.2 eV, which is sufficient to trigger defect

formation in the nanotube [21-24]. The presence of these defects can significantly lower the critical shell buckling load of the nanotube. Our simulations show that the presence of a single Stone-Wales defect reduces the critical shell buckling load from 58 *n*N to 43 *n*N. Stone-Wales defects can distort the sp^2 atomic arrangement, causing the walls of the SWCNT to become locally curved. Similarly, the presence of a single vacancy defect substantially reduces the structural stability of the nanotube, and the critical shell buckling load is lowered to about 48 *n*N. The effect of a single Stone-Wales defect and a single vacancy defect on the shell buckling profile of the nanotube is demonstrated in Fig. 5. For both defect types, observe that shell buckling initiates at the respective defect sites. In addition to lowering the critical shell buckling loads, it is also conceivable that the presence of both Stone-Wales and vacancy defects can substantially increase τ and hence $F(x_0)$: the increased cell wall curvature in the presence of Stone-Wales defects increases the frequency of collision of water molecules with the nanotube, while vacancy defects permit penetration of water molecules in the larger pore space, hence wetting the nanotube (transition from Cassie state to Wenzel state).

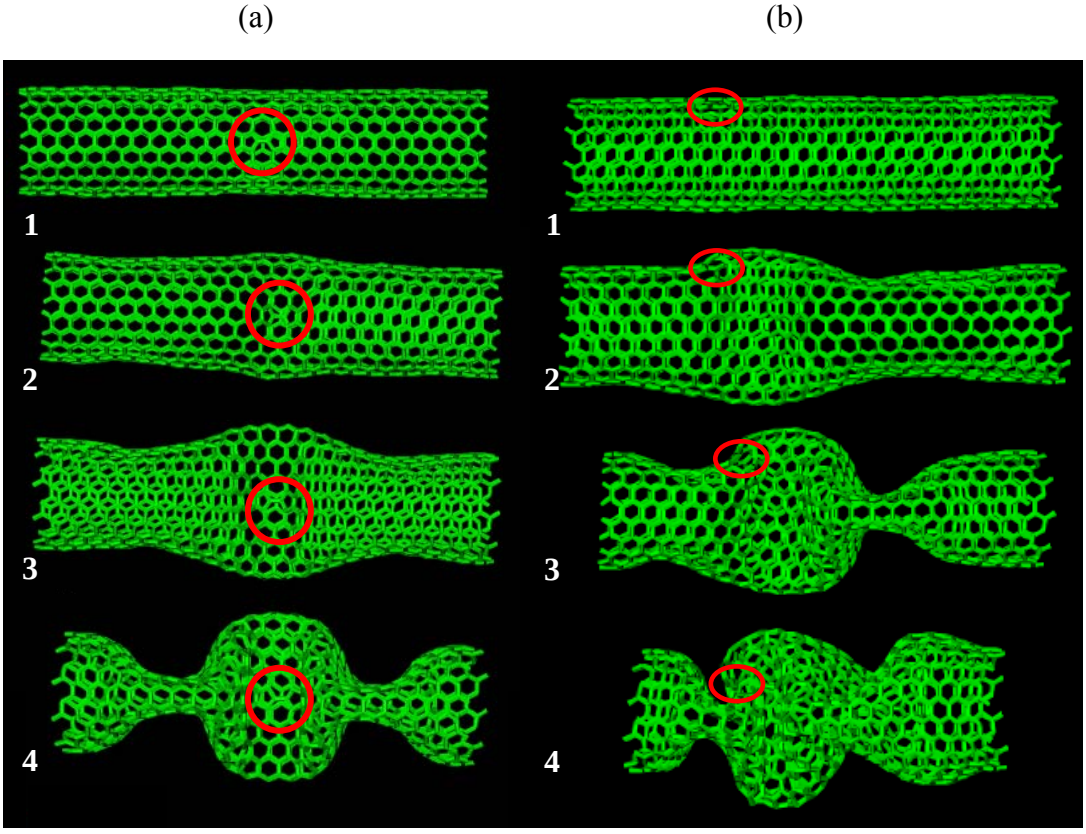

Figure 5. Time sequence of shell buckling profiles for (10,10) SWCNT containing a single (a) Stone-Wales defect and (b) vacancy defect. Encircled region denotes the defect location.

4. Conclusion

The mechanisms of nanotube scission under ultrasonication have been studied using scale-bridging molecular dynamics simulations. A calibration study was first performed to determine the frictional force distribution along the entire length of the SWCNT induced by streaming water flow during the implosion of cavitation bubbles. These accumulated frictional forces were subsequently imposed at the boundary ends of the scale-bridged model of a length-scale suitable for molecular dynamics calculations. We show that friction forces alone cannot account for the rapid nanotube scission observed experimentally [8, 9]. Our simulations suggest that the cutting of nanotubes is also attributed in-part to defect formation in the SWCNT induced by photon irradiation during multiple bubble sonoluminescence. The presence of these defects significantly increases the frictional stresses during streaming water flow along the nanotube, and at the same time lowers its critical shell buckling load.

Acknowledgement

The support of this work by the National University of Singapore under the Research Grant NUS-6-32254 is gratefully acknowledged.

References

[1] J-Y. Park, Y. Yaish, M. Brink, S. Rosenblatt, P.L. McEuen, Electrical cutting and nicking of carbon nanotubes using an atomic force microscope, Appl. Phys. Lett. 80 (2002), 4446-4448

[2] J. Lefebvre, J.F. Lynch, M. Llaguno, M. Radosavljevic, A.T. Johnson, Single wall carbon nanotube circuits assembled with an Atomic Force Microscope, Appl. Phys. Lett. 75 (1999), 3014-3016

[3] N. Yoneya, E. Watanabe, K. Tsukagoshi, Y. Aoyagi, Coulomb blockade in multiwalled carbon nanotube island with nanotube leads, Appl. Phys. Lett. 76 (2001), 1465-1467

[4] T.D. Yuzvinsky, A.M. Fennimore, W. Mickelson, C. Esquivias, A. Zettl, Precise cutting of nanotubes with a low-energy electron beam, Appl. Phys. Lett. 86 (2005), 053109

[5] I. Stepanek, G. Maurin, P. Bernier, J. Gavillet, A. Loiseau, R. Edwards, O. Jaschinski, Nano-mechanical cutting and opening of single wall carbon nanotubes, Chem. Phys. Lett. 331 (2000), 125-131

[6] G. Maurin, I. Stepanek, P. Bernier, J.-F. Colomer, J.B. Nagy, F. Henn, Segmented and opened multi-walled carbon nanotubes, Carbon 39 (2001), 1273-1278

[7] J. Liu, A.G. Rinzler, H. Dai, J.H. Hafner, R.K. Bradley, P.J. Boul, A. Lu, T. Iverson, K. Shelimov, C.B. Huffman, F. Rodriguez-Macias, Y-S. Shon, T.R. Lee, D.T. Colbert, R.E. Smalley, Fullerene Pipes, Science 280 (1998), 1253-1256

[8] D.A. Heller, R.M. Mayrhofer, S. Baik, Y.V. Grinkova, M.L. Usrey, M.S. Strano, Concomitant length and diameter separation of single-walled carbon nanotubes, J. Am. Chem. Soc. 126 (2004), 14567-14573

[9] F. Hennrich, R. Krupke, K. Arnold, J.A.R. Stütz, S. Lebedkin, T. Koch, T. Schimmel, M.M. Kappes, The mechanism of cavitation-induced scission of single-walled carbon nanotubes, J. Phys. Chem. B 111 (2007), 1932-1937

[10] C.E. Brennen, Cavitation and Bubble Dynamics, Oxford Univ. Press, 1995

[11] S.J. Plimpton, Fast Parallel Algorithms for Short-Range Molecular Dynamics, J. Comp. Phys. 117 (1995), 1-19

[12] S.J. Stuart, A.B. Tutein, J.A. Harrison, A reactive potential for hydrocarbons with intermolecular interactions, J. Chem. Phys. 112 (2000), 6472-6486

[13] H.W. Horn, W.C. Swope, J.W. Pitera, J.D. Madura, T.J. Dick, G.L. Hura, T. Head-Gordon, Development of an improved four-site water model for biomolecular simulations: TIP4P-Ew, J. Chem. Phys. 120 (2004), 9665-9678

[14] J.H. Walther, R. Jaffe, T. Halicioglu, P. Koumoutsakos, Carbon nanotubes in water: structural characteristics and energetics, J. Phys. Chem. B 105 (2001), 9980-9987

[15] H.J.C. Berendsen, J.P.M. Postma, W.F. van Gunsteren, A. DiNola, J.R. Haak, Molecular dynamics with coupling to an external bath, J. Chem. Phys. 81 (1984), 3684-3690

[16] E.M. Kotsalis, J.H. Walther, P. Koumoutsakos, Multiphase water flow inside carbon nanotubes, Int. J. Multiphase Flow 30 (2004), 995-1010

[17] I. Hanasaki, A. Nakatani, Flow structure of water in carbon nanotubes: Poiseuille type or plug-like, J. Chem. Phys. 124 (2006), 144708

[18] A. Poynor, L. Hong, I.K. Robinson, S. Granick, How water meets a hydrophobic surface, Phys. Rev. Lett. 97 (2006), 266101

[19] S. Granick, S, Motion and relaxations of confined liquids, Science 253 (1991), 1374-1379

[20] Y. Didenko, W.B. McNamara III, K.S. Suslick, K.S., The temperature of multi-bubble sonoluminescence in water, J. Phys. Chem. A 103 (1999), 10783-10788

[21] S. Suzuki, Y. Kobayashi, Threshold energy of low-energy irradiation damage in single-walled carbon nanotubes, J. Appl. Phys. 47 (2008), 2040-2043

[22] S. Okada, Energetics and electronic structure of carbon nanotubes with adatom-vacancy defects, Chemical Physics Letters 447 (2007), 263-267

[23] B.C. Pan, W.S. Yang, J. Yang, Formation energies of topological defects in carbon nanotubes, Phys. Rev. B 62 (2000), 12652

[24] L.G. Zhou, S-Q. Shi, Formation energy of Stone-Wales defects in carbon nanotubes, Appl. Phys. Lett. 83 (2003), 1222-1224